ACS APPLIED MATERIALS & INTERFACES

Research Article

www.acsami.org

# Oxasmaragdyrins as New and Efficient Hole-Transporting Materials for High-Performance Perovskite Solar Cells

Sandeep B. Mane,[†,#] Albertus Adrian Sutanto,[†,‡,§,#] Chih-Fu Cheng,[†] Meng-Yu Xie,[†,∥] Chieh-I Chen,[†] Mario Leonardus,[†] Shih-Chieh Yeh,[†] Belete Bedemo Beyene,[†] Eric Wei-Guang Diau,[⊥] Chin-Ti Chen,[†] and Chen-Hsiung Hung*[,†]

[†]Institute of Chemistry, Academia Sinica, Taipei 11529, Taiwan

[‡]Department of Chemical Engineering, National Taiwan University of Science and Technology, Taipei 10607, Taiwan

[§]Department of Chemical Engineering, Faculty of Engineering, Diponegoro University, Semarang 50275, Indonesia

[∥]Department of Chemistry and Biochemistry, National Chung Cheng University, Chiayi 62102, Taiwan

[⊥]Department of Applied Chemistry, National Chiao Tung University, Hsinchu 30010, Taiwan

Supporting Information

**ABSTRACT:** The high performance of the perovskite solar cells (PSCs) cannot be achieved without a layer of efficient hole-transporting materials (HTMs) to retard the charge recombination and transport the photogenerated hole to the counterelectrode. Herein, we report the use of boryl oxasmaragdyrins (SM01, SM09, and SM13), a family of aromatic core-modified expanded porphyrins, as efficient hole-transporting materials (HTMs) for perovskite solar cells (PSCs). These oxasmaragdyrins demonstrated complementary absorption spectra in the low-energy region, good redox reversibility, good thermal stability, suitable energy levels with $CH_3NH_3PbI_3$ perovskite, and high hole mobility. A remarkable power conversion efficiency of 16.5% ($V_{oc}$ = 1.09 V, $J_{sc}$ = 20.9 mA cm$^{-2}$, fill factor (FF) = 72%) is achieved using SM09 on the optimized PSCs device employing a planar structure, which is close to that of the state-of-the-art hole-transporting materials (HTMs), spiro-OMeTAD of 18.2% ($V_{oc}$ = 1.07 V, $J_{sc}$ = 22.9 mA cm$^{-2}$, FF = 74%). In contrast, a poor photovoltaic performance of PSCs using SM01 is observed due to the interactions of terminal carboxylic acid functional group with $CH_3NH_3PbI_3$.

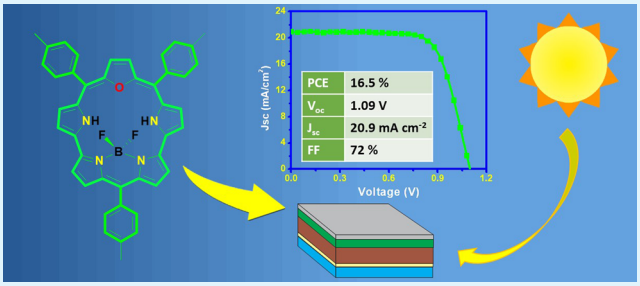


**KEYWORDS:** *porphyrin, boryl oxasmaragdyrin, core modification, hole-transporting material, perovskite solar cells*

## 1. INTRODUCTION

Organometal halide perovskite solar cells (PSCs) have emerged as a game changer in the thin-film photovoltaic technologies, witnessing a rapid growth in the past few years.[1−3] Along with impressive efficiencies and cost-effective processing, these perovskites also possess excellent optical properties,[4] ambipolar charge transport properties,[5] and adequate electron−hole diffusion lengths.[6,7] Furthermore, the performance of these perovskite materials can be fine-tuned easily by compositional and structural manipulation,[8−10] $TiO_2$ nanostructure modification,[11] and appropriate choice of hole-transporting material (HTM).[2,12] The overall photon-to-current conversion efficiencies of these perovskite solar cells have climbed sharply from less than 10 to 22.1% in just 5 years.[13] HTMs play a significant role in PSCs to achieve both long-term stability and enhanced power conversion efficiencies (PCEs). Besides state-of-the-art 2,2′,7,7′-tetrakis(*N*,*N*-di-*p*-methoxyphenylamine)-9,9′-spirofluorene (spiro-OMeTAD), various small molecules,[12,14−20] polymers,[3,12] phthalocyanines (Pcs),[21−31] porphyrins,[32−34] and inorganic materials[35,36] have been used as HTMs. The best PCEs have been obtained by incorporating only spiro-OMeTAD[17] or poly(triaryl amine) (PTAA)[3] as the solid-state HTM. Despite the high performance of spiro-OMeTAD and PTAA, they suffer from high-cost synthesis, difficult purification, and low stability, which may hinder their application in a larger scale.[22,37,38]

Porphyrins and phthalocyanines (Pcs) have emerged as effective molecules to be used as HTMs in PSCs. Kumar et al. have applied CuPc as a low-cost HTM in PSCs to obtain the PCE of 5%.[21] In another report, Ramos and co-workers have used a nonaggregated Zn(II)[octa(2,6-diphenylphenoxy)-phthalocyanine] (TT80) as an HTM in the PSC device to obtain a PCE of 6.7%.[22] Subphthalocyanine has also been utilized as an HTM in PSCs giving the PCE of 6.6%.[39] Nanorod-like CuPc also has been incorporated as an HTM in the carbon counterelectrode-based PSCs to obtain a higher

Received: July 6, 2017
Accepted: August 29, 2017
Published: August 29, 2017





DOI: 10.1021/acsami.7b09803
ACS Appl. Mater. Interfaces 2017, 9, 31950−31958

**Scheme 1. Molecular Structures of SM HTMs**

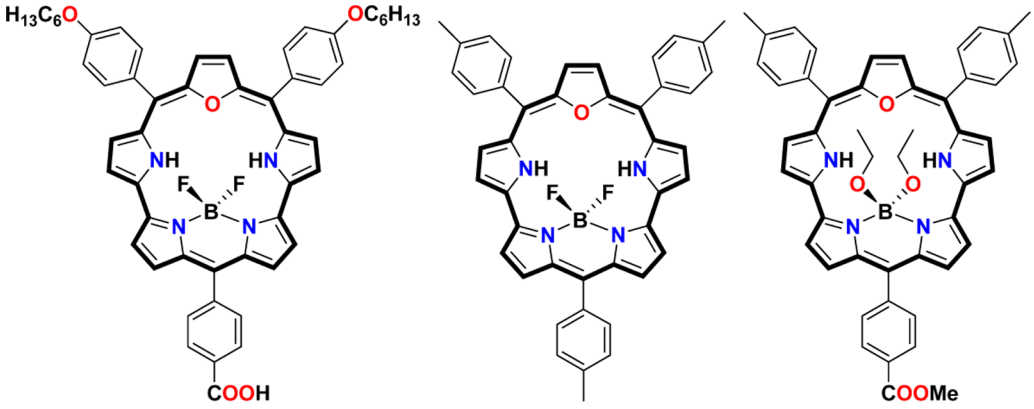


**Scheme 2. Synthetic Pathway for SM HTMs**[a]

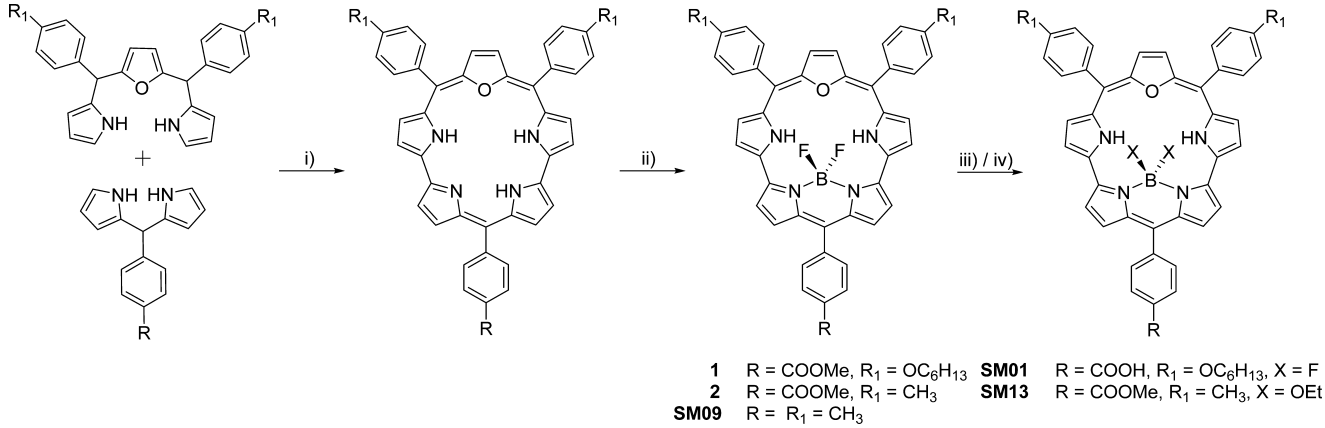


[a]Reactions and conditions: (i) trifluoroacetyl, 2,3-dichloro-5,6-dicyano-1,4-benzoquinone, dichloromethane; (ii) $NEt_3$, $BF_3OEt_2$; for SM01 (iii) aq KOH, tetrahydrofuran (THF); for SM13 (iv) EtOH, $AlCl_3$.

PCE of 16.1%.[40] Very recently, nickel phthalocyanine combined with vanadium(V) oxide ($V_2O_5$) have been successfully applied in mesoscopic PSCs to achieve a PCE of 16.8%.[23] The highest efficiency of phthalocyanine-based HTMs of 17.5% was obtained by employing tetra-5-hexylthiophene-based ZnPc in the mesoscopic PSCs device.[31] In 2016, Yeh's group reported HTMs based on the zinc porphyrin−ethylaniline conjugates on the mesoscopic PSCs devices employing $CH_3NH_3PbI_3$ perovskite.[33] A comparable performance to spiro-OMeTAD with PCE of 16.6% was achieved for PSCs based on *n*-butyl tethered Y2.[33] Recently, Chen and co-workers reported arylamine-substituted porphyrins as HTMs on the mesoscopic PSCs devices employing $CH_3NH_3PbI_3$ perovskite yielding a PCE of 17.78%.[34] Noticeably, there is no report on applying expanded porphyrins as HTMs in PSCs till now.

Boryl oxasmaragdyrins, an expanded core-modified porphyrins, have recently gained much attention as low-energy sensitizers in dye-sensitized solar cells due to their impressive optical properties, step-economic synthesis, high overall yields, and panchromatic light-harvesting ability.[41,42] A very impressive PCE of 5.7% in this family of core-modified sensitizers has been achieved by our group.[41] During the studies, we also noticed that the highest occupied molecular orbital−lowest unoccupied molecular orbital (HOMO−LUMO) energy levels of these expanded core-modified porphyrins match perfectly with the requirements for the HTM in PSCs. Moreover, boryl oxasmaragdyrins offer many advantages, such as simpler synthesis and purification processes, low cost, and moisture stability. Herein, we report the first application of these boryl oxasmaragdyrins as HTMs in PSCs.

## 2. RESULTS AND DISCUSSION

**2.1. Molecular Design and Synthesis.** The molecular structures of the studied SM HTMs are depicted in Scheme 1. SM01 consists of two hexyloxyphenyl groups and one carboxyphenyl group on the meso-position, whereas SM09 comprised of three tolyl groups at the meso-positions. In SM13, other than a methylbenzoate derivative, the fluoride groups on the boron center are replaced by ethoxy groups to manipulate the electronegativity. The synthetic pathway for these SM molecules is depicted in Scheme 2. SM01 and SM13 have been reported by our group previously,[41,42] and SM09 is prepared by following the literature procedure.[43] Owing to the planar porphyrin ring, these molecules are expected to have enhanced intermolecular $\pi$-stacking, which might be helpful for an efficient hole transport. For the synthesis of SM HTMs, the corresponding 16-oxatripyrrane and dipyrromethane were condensed following McDonalds "3 + 2" protocol to yield free-base oxasmaragdyrins, which on further treatment with excess trimethylamine and boron trifluoride etherate gave boryl


DOI: 10.1021/acsami.7b09803
ACS Appl. Mater. Interfaces 2017, 9, 31950−31958

oxasmaragdyrins (1, 2, and SM09). For SM01, compound 1 is treated with aqueous KOH to convert ester group into acid, whereas compound 2 is reacted with aluminum trichloride in excess ethanol to obtain SM13.

**2.2. Optical, Electrochemical, and Hole-Transporting Properties.** As seen from the absorption spectra in Figure 1a,

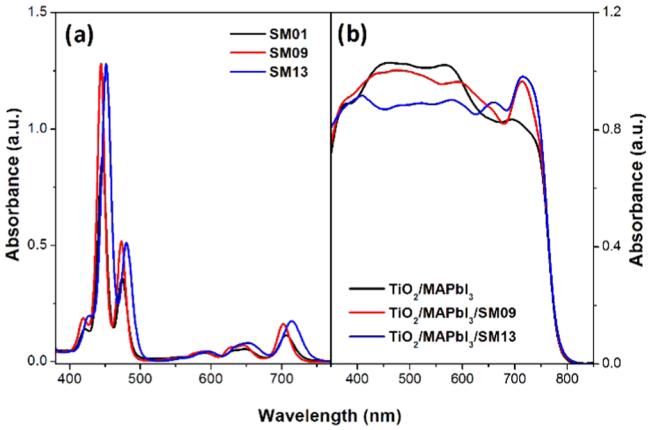


**Figure 1.** UV−visible spectra of SM HTMs (a) in THF and (b) as thin films.

these boryl oxasmaragdyrins show two intense split Soret bands in the 450−550 nm region and Q bands in the 600−800 nm region. The split Soret band is a characteristic phenomenon of boryl oxasmaragdyrin, and the UV−vis spectra of these compounds are consistent with other literature-reported boryl oxasmaragdyrin.[43] The thin-film UV−vis spectra measured using an integrating sphere on the HTM layer coated $MAPbI_3$ film with the thickness of 50, 100, 200, and 180 nm for $TiO_2$ compact layer (c-$TiO_2$), $TiO_2$ mesoporous layer (mp-$TiO_2$) infiltrated with $MAPbI_3$, overcapping $MAPbI_3$, and oxasmaragdyrin, respectively, are presented in Figure 1b. The distinctive feature with an enhancement on the absorbance between 650 and 800 nm for the perovskite films coated with a boryl oxasmaragdyrin suggests the potential of using these oxasmaragdyrins as a cosensitizing dye to absorb the low-energy near-IR photons under a proper band gap alignment.

The highest occupied molecular orbital (HOMO) and the lowest unoccupied molecular orbital (LUMO) of these boryl oxasmaragdyrins were determined directly by cyclic voltammetry (CV). As depicted in Figure 2a and Table 1, two reversible oxidation waves and one reversible reduction wave were observed for SM01 and SM09, whereas two reversible oxidation and two reversible reduction waves were observed for SM13. The energy level diagram (Figure 2b) with HOMO and LUMO energy levels converted directly from the first oxidation potential and the first reduction potential, respectively, on the cyclic voltammograms is plotted to gain further insight into the feasibility of using boryl oxasmaragdyrin to mediate hole migration. As seen from the energy level diagram, all of the HOMO energy levels of SMs are more positive than that of perovskite methylammonium lead iodide ($MAPbI_3$) but more negative than the HOMO energy level of spiro-OMeTAD, suggesting that these boryl oxasmaragdyrins can be effective materials for hole transporting on the $MAPbI_3$-based perovskite solar cells. Noticeably, the HOMO and LUMO potentials of SM13 are shifted to more positive values after the substitution of electron-donating ethoxy groups on the boron center.

The hole mobility of the boryl oxasmaragdyrins was determined by using space-charge-limited currents (SCLCs) following the literature procedures at room temperature.[44−46] Because of its poor PCE (vide infra), we did not check the hole mobility of SM01. The devices coated with hole-migration materials only, ITO/PEDOT:PSS/HTM/Al, were fabricated to perform the SCLC measurement. The zero field hole mobility ($\mu_h$) of pristine spiro-OMeTAD is $1 \times 10^{-5}$ $cm^2/(V\ s)$, which is similar to $\sim 1.8 \times 10^{-5}$ $cm^2/(V\ s)$ reported in the literature.[44] For pristine SM09 and SM13, our measurements obtained $\mu_h$ of $1.6 \times 10^{-6}$ and $2 \times 10^{-8}$ $cm^2/(V\ s)$, respectively. However, with the addition of LiTFSI and *t*BP to the solution of boryl oxasmaragdyrins for the preparation of a SM film, the $\mu_h$ was increased substantially to $2.8 \times 10^{-4}$, $1.7 \times 10^{-4}$, and $1.7 \times 10^{-6}$ $cm^2/(V\ s)$ for spiro-OMeTAD, SM09, and SM13 respectively. Figure 3 shows the electric field ($E^{1/2}$) dependent hole mobility

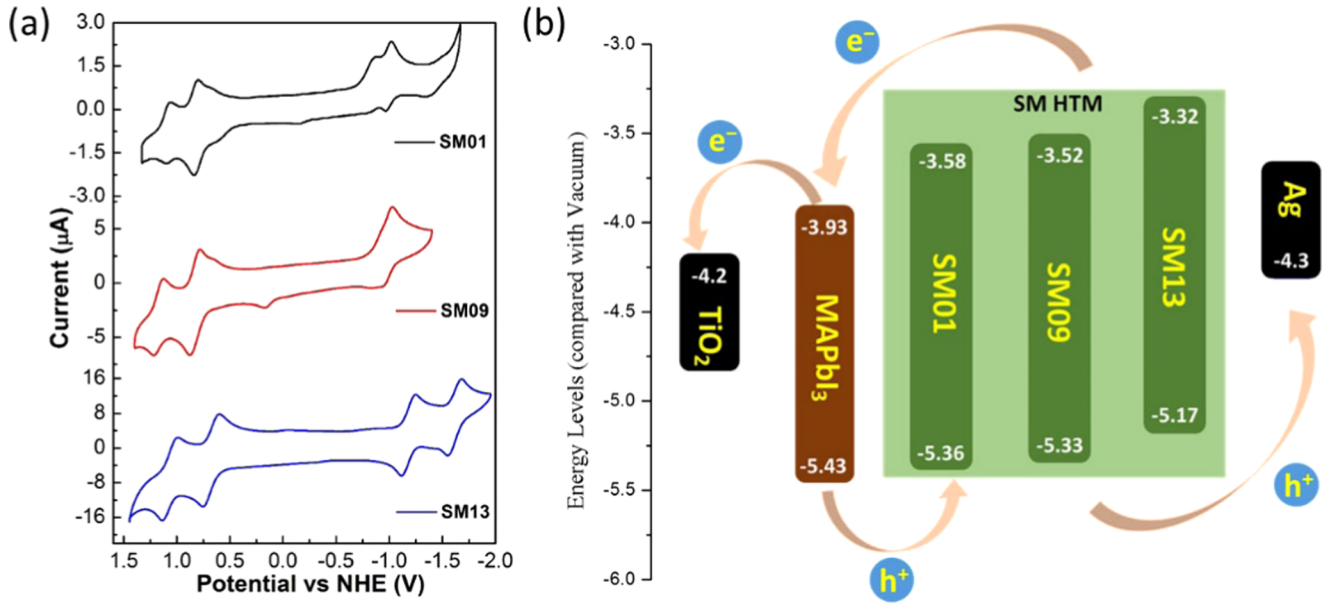


**Figure 2.** (a) CV spectra for SM molecules and (b) energy level diagram for SM HTMs.



DOI: 10.1021/acsami.7b09803
ACS Appl. Mater. Interfaces 2017, 9, 31950−31958

**Table 1. Optical and Electrochemical Data of SM HTMs**

| HTM | $\lambda_{max}$ (nm)[a] | $E_{1/2}$ (V)[b] first ox | second ox | first red | band gap (eV) | HOMO[c] (eV) | LUMO[c] (eV) |
|---|---|---|---|---|---|---|---|
| SM01 | 446, 474, 706 | 0.86 | 1.18 | −0.92 | 1.78 | −5.36 | −3.58 |
| SM09 | 444, 473, 702 | 0.83 | 1.17 | −0.98 | 1.81 | −5.33 | −3.52 |
| SM13 | 451, 480, 714 | 0.67 | 1.06 | −1.18 | 1.85 | −5.17 | −3.32 |

[a]Absorption maximum of SM HTMs in THF. [b]CV measurements were carried out in THF with $TBAPF_6$ (0.1 M) as the supporting electrolyte and ferrocene/ferrocenium ($Fc/Fc^+$) as the internal reference. [c]CV potentials were converted to the vacuum scale according to the formula of $E_{HOMO} = -(E_{ox} + 4.5)$ (eV) and $E_{LUMO} = -(E_{red} + 4.5)$ (eV).

($\mu_h$) of three HTMs, with (Figure 3b) and without (Figure 3a) LiTFSI and *t*BP additions.

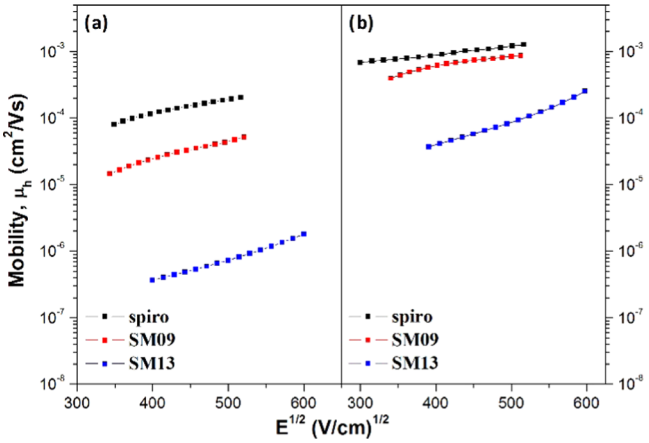


**Figure 3.** Electric field ($E^{1/2}$) dependent $\mu_h$ of HTMs, without (a) and with (b) LiTFSI and *t*BP addition.

**2.3. Performance of Perovskite Solar Cells.** *2.3.1. Mesoscopic Device Structure.* The composition of the studied PSC devices is displayed in Figure 4, where a compact $TiO_2$ layer was deposited on a fluorine-doped tin oxide−coated glass by spray pyrolysis as a hole-blocking layer. A mesoporous $TiO_2$ layer was spin-coated onto the fluorine-doped tin oxide (FTO)/c-$TiO_2$ layer. The $MAPbI_3$ solution was then spin-coated on the FTO/c-$TiO_2$/mp-$TiO_2$ substrate. During the spin-coating process, dry chlorobenzene was added as the antisolvent to the substrate after a short delay. Then, the films were annealed at 100 °C for 10 min. The color of the annealed film changed from transparent to dark brown, indicating the crystallization of the $MAPbI_3$ layer. The SM HTM layer was then introduced by spin-coating, and finally silver contact electrode was deposited by thermal deposition as a back electrode. From the cross-sectional SEM image of the device with SM09 as the HTM (Figure 4), the layer thickness of each component of the device was determined. A 50 nm c-$TiO_2$, 100 nm mesoporous $TiO_2$ infiltrated with $MAPbI_3$, 200 nm of overcapping $MAPbI_3$, an HTM layer of 180 nm, and finally a silver electrode of 80 nm were assigned.

The current−voltage ($J$−$V$) characteristics of the perovskite solar cells assembled with SM molecules as the HTM measured under 100 mW/cm$^2$ photon flux (AM 1.5G) are displayed in Figure 5, and the corresponding photovoltaic parameters are summarized in Table 2. The PCEs of 4.9, 14.5, and 14.1% were obtained for SM01, SM09, and SM13, respectively. Reference cells with spiro-OMeTAD HTM are also prepared for comparison. Under similar measurement conditions, the average of 10 devices with spiro-OMeTAD as HTM shows a short-circuit current density ($J_{sc}$) of 21.1 mA cm$^{-2}$, an open-circuit voltage ($V_{oc}$) of 1.02 V, and a fill factor (FF) of 69%, leading to an average PCE of 14.8%. Among the three boryl oxasmaragdyrins, SM01 showed an unusually poor performance in stark contrast with the high efficiency of SM09 and SM13. The best device with SM01 as HTM obtained PCE of 4.9% based on $J_{sc}$ of 9.9 mA cm$^{-2}$, $V_{oc}$ of 0.83 V, and FF of 59%. We believe that this lower performance of SM01 is due to the interactions of terminal carboxylic acid with the $MAPbI_3$ layer, making the device very unstable, confirmed by the continuing color fading of the $MAPbI_3$ layer. However, we did not observe such color fading even after a month when the devices were assembled with SM09 or SM13 as HTM. The champion device with SM09 as HTM shows $J_{sc}$ of 20.5 mA cm$^{-2}$, $V_{oc}$ of 1.01 V, FF of 70%, and PCE of 14.5%. It is worth noting that, as shown in Figure 5a, the photocurrent density for SM09 is the same as that of the highest-efficiency PSC device using spiro-OMeTAD as the HTM, whereas the open-circuit voltage and the fill factor are slightly lower. The best device with SM13 as the HTM

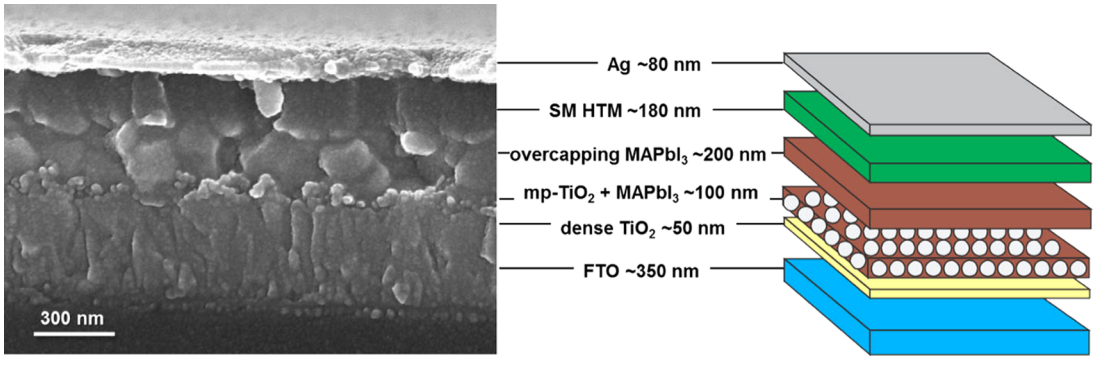


**Figure 4.** Composition of the device with SM HTM.


DOI: 10.1021/acsami.7b09803
ACS Appl. Mater. Interfaces 2017, 9, 31950−31958

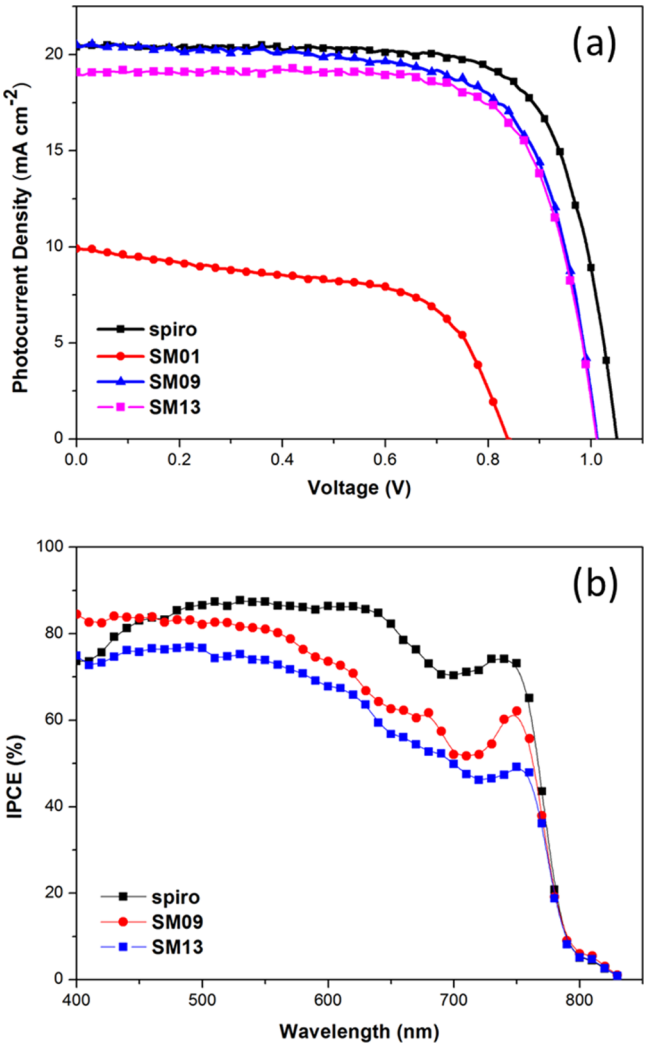


**Figure 5.** a) $J$–$V$ characteristics and (b) incident photon-to-current conversion efficiency (IPCE) spectra of perovskite solar cells assembled with SM HTMs and spiro-OMeTAD (best cell) measured under standard 1 sun conditions.

shows $J_{sc}$ of 19.1 mA cm$^{-2}$, $V_{oc}$ of 1.01 V, FF of 73%, and PCE of 14.1%.

It is also noticed that the $J_{sc}$ for SM13 is slightly lower than that for SM09, resulting in a slightly lower PCE. The better performance of the SM09 compared with SM13 is well in accordance with the hole mobility data. The statistical data for ten best devices based on all of the three SMs as HTM is given in Tables S1–S3. The trends in the $J$–$V$ curves can be well understood from the incident photon-to-current conversion efficiency (IPCE) spectra. The best device with spiro-OMeTAD as the HTM displayed a very broad IPCE plateau of over 80%, covering the whole visible region, as displayed in Figure 5b. The IPCE spectra of the SM molecules are in qualitative agreement with the corresponding absorption spectra of the thin films (Figure 2b). The device with SM09 as the HTM also showed a much higher IPCE value (80%) of up to 600 nm and then decreases to 60% in the 600–800 nm region. The device with SM13 as the HTM shows slightly lower IPCE values compared with SM09, with the IPCE plateau in the range of 50–70% in the whole visible region.

*2.3.2. Planar Device Structure with $SnO_2$ as Electron-Transporting Materials.* Device optimization was carried out for the best-performing HTM, SM09, by preparing a planar device configuration employing $SnO_2$ as the electron-transporting layer instead of $TiO_2$. The planar device configuration employing $SnO_2$ was chosen because it offers a low-temperature process and an easier fabrication step without the application of the mesoscopic structure, which is important for a large-scale fabrication process. A thin layer of $SnO_2$ was deposited on top of the FTO glass according to the reported procedure with some modifications.[47] The optimized planar device structure is displayed in the SEM image shown in Figure 6.

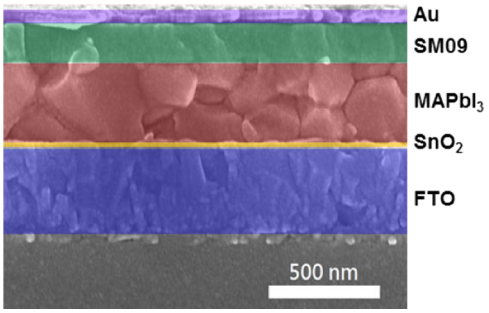


**Figure 6.** Cross-sectional SEM images of the optimized planar device employing SM09 (FTO/$SnO_2$/$MAPbI_3$ perovskite/SM09/Au).

The current–voltage ($J$–$V$) characteristics of PSCs with SM09 prepared under the optimized condition are displayed in Figure 7, and the corresponding photovoltaic parameters are summarized in Table 3. PSC devices using spiro-OMeTAD were also fabricated using the optimized method under the same condition as a comparison. The optimized device employing SM09 achieved a pretty significant improvement in the overall photovoltaic performance with $J_{sc}$ of 20.9 mA cm$^{-2}$, $V_{oc}$ of 1.09 V, FF of 72%, and PCE of 16.5%. The high performance of the optimized devices is well supported with the IPCE spectra depicted in Figure 8. The IPCE values, lying

**Table 2. Photovoltaic Parameters for the Devices with SM HTMs**

| HTM | | $J_{sc}$ (mA cm$^{-2}$) | $V_{oc}$ (V) | FF (%) | PCE (%) |
|---|---|---|---|---|---|
| spiro-OMeTAD | average | 21.1 | 1.02 | 69 | 14.8 |
| | best | 21.6 | 1.05 | 74 | 15.8 |
| SM01 | average | 9.3 | 0.71 | 60 | 4.0 |
| | best | 9.9 | 0.83 | 59 | 4.9 |
| SM09 | average | 19.1 | 0.99 | 70 | 13.3 |
| | best | 20.5 | 1.01 | 70 | 14.5 |
| SM13 | average | 17.7 | 0.96 | 71 | 12.2 |
| | best | 19.1 | 1.01 | 73 | 14.1 |


DOI: 10.1021/acsami.7b09803
ACS Appl. Mater. Interfaces 2017, 9, 31950–31958

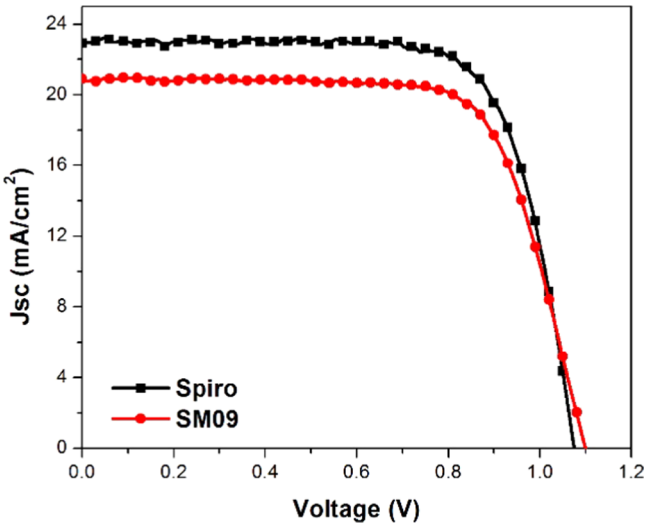


**Figure 7.** $J$–$V$ curves for the optimized devices.

**Table 3. Photovoltaic Parameters for the Optimized Devices with spiro-OMeTAD and SM09**

| HTM | $J_{sc}$ (mA cm$^{-2}$) | $V_{oc}$ (V) | FF (%) | PCE (%) |
|---|---|---|---|---|
| spiro-OMeTAD | 22.9 | 1.07 | 74 | 18.2 |
| SM09 | 20.9 | 1.09 | 72 | 16.5 |

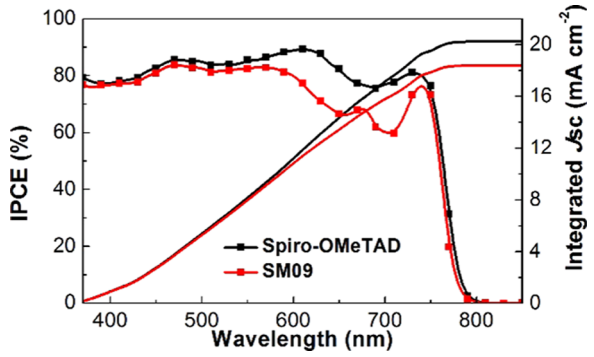


**Figure 8.** IPCE spectra for the optimized devices.

above 70% in most of the wavelength range, have improved significantly from the aforementioned $TiO_2$ mesoscopic device using the same SM09 as the HTM. The histogram and the statistical data of the photovoltaic parameters of the optimized devices employing SM09 are shown in Figure S5 and Table S6, giving the average PCE of 14.4% over 25 devices. The enhancement in photovoltaic performance is due to the higher electron mobility and the more negative conduction band of $SnO_2$ compared with $TiO_2$.[47,48] These characteristics of $SnO_2$ will enhance the photoelectron injection, extraction, and collection from the perovskite layer.[48]

To have a comparison of the device stability, we carried out the stability test of optimized $SnO_2$ planar perovskite devices with SM09 and spiro-OMeTAD as the HTM. The non-encapsulated devices were stored for 40 days inside the nitrogen glovebox, and the PCEs were measured periodically under the ambient conditions. Figure 9 shows the monitored PCEs data of the optimized devices. After 40 days, the device employing SM09 still retains 85% of its initial PCE, which is comparable to the device employing spiro-OMeTAD that retains 90% of its initial PCE.

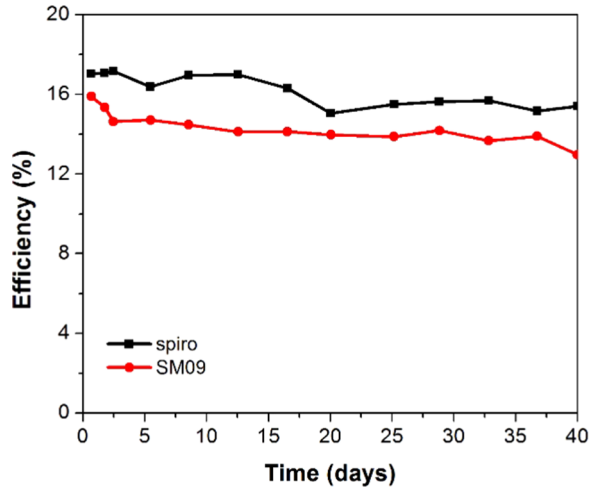


**Figure 9.** Preliminary stability test of the optimized device employing spiro-OMeTAD and SM09.

## 3. CONCLUSIONS

In summary, we have demonstrated for the first time that core-modified expanded porphyrins can be successfully applied as efficient hole-transporting materials in perovskite solar cells. These boryl oxasmaragdyrins exhibit low-energy Q-bands, which is complementary with the absorption spectrum of $MAPbI_3$ perovskite solar cells. Boryl oxasmagdyrins also demonstrated good redox reversibility, good thermal stability, suitable energy levels, and high hole mobility. The optimized device with SM09 as the HTM achieves a power conversion efficiency of 16.5%, with a photocurrent density of 20.9 mA cm$^{-2}$, an open-circuit voltage of 1.09 V, and a fill factor of 72%. The performance of SM09 is comparable to that of the state-of-the-art HTM spiro-OMeTAD. Moreover, boryl oxasmaragdyrins also offer many advantages, such as simpler synthesis and purification processes, low cost, and moisture stability. This high performance from boryl oxasmaragdyrins will open a new path for the screening of a vast library of expanded porphyrin derivatives for photovoltaic applications.

## 4. EXPERIMENTAL SECTION

**4.1. General Methods.** All of the chemicals used for the synthesis were purchased from commercial sources and used as such without further purification. Unless otherwise mentioned, the reactions were carried out in inert atmosphere. Dry solvents used for the synthesis were dried using PureSolv MD 5 system (Innovative Technology, Inc). Basic alumina (63–200 $\mu$m, Merck) and silica gel (40–63 $\mu$m, Merck) were used for purifications by column chromatography. Merck silica gel plates were used for thin-layer chromatography analysis. Bruker Avance 400 FT and DRX 500 spectrometers were used for NMR analysis. electrospray ionization (ESI) ion trap mass spectra were recorded using Finnigan MAT LCQ mass spectrometer, whereas JMS-700 double-focusing mass spectrometer was used for HR-FAB spectra. JASCO V-670 UV–vis/near-infrared spectrophotometer was used to record UV–vis absorption spectra of the SMs in a solvent and as thin films, respectively. The CV measurements were recorded on CHI 621B electrochemical analyzer (CH Instruments, Austin, TX) in a degassed THF with $Bu_4NPF_6$ as the supporting electrolyte. A glassy carbon as the working electrode, a silver wire as the pseudoreference electrode, and a platinum wire as the auxiliary electrode were used for the cell. Ferrocene$^{+1/0}$ redox couple was used as the internal standard with 50 mV/s scan rate and the potential values were converted to the vacuum scale.

**4.2. Synthesis.** The boryl oxasmaragdyrins used in this study were prepared by following the literature methods. The synthesis of SM01



DOI: 10.1021/acsami.7b09803
ACS Appl. Mater. Interfaces 2017, 9, 31950–31958

and SM13 has been reported previously by our group,[41,42] whereas SM09 was synthesized following the literature protocols.[43]

**4.3. SM09.** $^{1}$H NMR (400 MHz, $CDCl_3$) $\delta$ = −3.58 (t, 2H; −NH), 2.78 (s, 9H; $-CH_3$), 7.69 (d, 4H, $J$ = 8 Hz; Ph), 7.78 (d, 2H, $J$ = 8 Hz; Ph), 8.28 (d, 4H, $J$ = 8 Hz; Ph), 8.49 (d, 2H, $J$ = 8.28 Hz; Ph), 8.94 (d, 2H, $J$ = 4.04; $\beta$-pyrr), 9.43 (s, 2H; $\beta$-fur), 9.56 (d, 2H, $J$ = 4.02 Hz, $\beta$-pyrr), 10.16 (d, 2H, $J$ = 4.03; $\beta$-pyrr), 10.24 (d, 2H, $J$ = 4.04 Hz; $\beta$-pyrr) ppm; $^{11}$B NMR (128.3 MHz, $CDCl_3$) $\delta$ = −12.32 (br s) ppm; $^{19}$F NMR (376.376 MHz, $CDCl_3$) $\delta$ = −149.34 (br s) ppm; $^{13}$C NMR (100 MHz, $CDCl_3$) $\delta$ = 149.86, 139.65, 138.00, 137.86, 136.15, 134.67, 134.25, 131.91, 131.03, 130.61, 129.18, 128.31, 124.87, 124.62, 123.68, 121.56, 120.32, 119.92, 106.84, 21.63, 21.54 ppm; HRMS-ESI: $m/z$ calcd for $C_{44}H_{33}BF_2N_4ONa$: 705.2613, found 705.2618 $[M + Na]^+$.

**4.4. Perovskite Solar Cell Device Fabrication.** FTO-coated glass substrates (TEC-15, Solaronix) were patterned by chemical etching with Zn powder and 2 M HCl in the aqueous solution. The etched substrate was then cleaned with Extran MA 02 (Merck) and ultrasonically cleaned with deionized water, acetone, and 2-propanol in that sequence for 10 min, respectively. After drying under an $N_2$ stream, the substrates were further cleaned by an $O_2$ plasma cleaner. A dense layer of $TiO_2$ was then coated on the substrates by spray pyrolysis of titanium diisopropoxide bis(acetyl acetonate) diluted in absolute ethanol at a volumetric ratio of 1:20 at 500 °C. Oxygen was used as the carrier gas for spray pyrolysis deposition. The glass substrates were kept at 500 °C for 30 min after spray pyrolysis deposition process. A mesoporous layer of $TiO_2$ was deposited by spin-coating $TiO_2$ diluted in absolute ethanol at 1:12 weight ratio at 5000 rpm for 30 s to get 100 nm thick mp-$TiO_2$ layer. The thickness of mp-$TiO_2$ was adjusted by varying the $TiO_2$ paste concentration in ethanol at 1:14, 1:8, and 1:4 weight ratio to get 60, 200, and 300 nm thick mp-$TiO_2$ layer, respectively. The layer was then heated at 180 °C for 5 min, followed by annealing at 550 °C for 30 min in air to remove organic components. Perovskite and HTM layer depositions were carried out inside the nitrogen glovebox. The perovskite precursor solution was prepared by mixing 200 mg of the synthesized $CH_3NH_3I$ and 578 mg of lead(II) iodide (99.9%, Alfa Aesar) in 1 mL anhydrous $N$,$N$-dimethylformamide by stirring at 70 °C overnight to obtain a clear yellow $CH_3NH_3PbI_3$ solution with a concentration of 45 wt %. An 80 $\mu$L of $CH_3NH_3PbI_3$ solution was spin-coated on an FTO glass substrate coated with a mesoporous layer of $TiO_2$ and a dense layer of $TiO_2$ at 5000 rpm for 30 s. For the planar device, the dense layer of $SnO_2$ was prepared by spin-coating 0.1 M tin(II) chloride dihydrate in ethanolic solution at 3000 rpm for 30 s, followed by annealing at 185 °C for 1 h. $CH_3NH_3PbI_3$ layer was deposited directly on top of $SnO_2$ layer under the same condition as the mesoscopic device. After a specific delay time of 4 s, for the optimized condition, in the spin-coating process, a 240 $\mu$L of anhydrous chlorobenzene was quickly dropped at the center of the substrate. The addition of chlorobenzene will change the color of the substrate instantaneously from transparent to light brown. The substrate was then heated at 100 °C for 10 min on a hot plate to remove the remaining solvent. During heating, the color of perovskite layer changed from light brown to dark brown. 67 mM of hole-transporting material was prepared by dissolving spiro-OMeTAD, SM01, SM09, and SM13, respectively, in chlorobenzene. Then, 27 mM of LiTFSI and 147 mM of $t$BP were added as additives to the above solution. The solution was then spin-coated at 2200 rpm for 30 s. Finally, an 80 nm thick silver counterelectrode was deposited under high vacuum ($<8 \times 10^{-6}$ Torr) by thermal evaporation.

**4.5. Device Characterization.** Current−voltage characteristics were measured by using a solar simulator (Newport, Oriel Instruments, 91160A) with a source meter (Keithley 2400) at the light intensity of 100 mW/cm$^2$, AM 1.5 G illumination. A Si-reference cell (Newport, Oriel Instruments, 91150) certified by NREL was used to calibrate output of the light source of the solar simulator. A metal mask with an aperture of 9 mm$^2$ was used during measurement to define the active area of the perovskite solar cells. Incident photon-to-electron conversion efficiency (IPCE) was measured using a power source (Newport, 300 W xenon lamp) with a monochromator (Newport, Cornerstone 260). The IPCE spectra were recorded under the short-circuit condition using a Keithley 2401 source meter. The cross-sectional morphology and the surface morphology of perovskite solar cells were investigated using field-emission scanning electron microscope (FE-SEM), Zeiss Ultra Plus.

## ■ ASSOCIATED CONTENT

### Supporting Information

The Supporting Information is available free of charge on the ACS Publications website at DOI: 10.1021/acsami.7b09803.

Space-charge-limited current (SCLC) characterization method, statistical and photovoltaic data of devices employing SM HTMs, TGA plots, cross-sectional SEM image of the SM13 device (PDF)

## ■ AUTHOR INFORMATION


### Corresponding Author

*E-mail: chhung@gate.sinica.edu.tw.

### ORCID

Eric Wei-Guang Diau: 0000-0001-6113-5679

Chen-Hsiung Hung: 0000-0002-8060-348X


### Author Contributions

#S.B.M. and A.A.S. contributed equally.

### Notes

The authors declare no competing financial interest.

## ■ ACKNOWLEDGMENTS

We acknowledge the financial assistance from the Ministry of Science and Technology (MOST) and Academia Sinica. Technical support from the advanced nano/micro-fabrication and characterization lab at Academia Sinica is also acknowledged.

## ■ REFERENCES


(1) Green, M. A.; Ho-Baillie, A.; Snaith, H. J. The Emergence of Perovskite Solar Cells. *Nat. Photonics* **2014**, *8*, 506−514.

(2) Kazim, S.; Nazeeruddin, M. K.; Grätzel, M.; Ahmad, S. Perovskite as Light Harvester: A Game Changer in Photovoltaics. *Angew. Chem., Int. Ed.* **2014**, *53*, 2812−2824.

(3) Yang, W. S.; Noh, J. H.; Jeon, N. J.; Kim, Y. C.; Ryu, S.; Seo, J.; Seok, S. I. High-Performance Photovoltaic Perovskite Layers Fabricated through Intramolecular Exchange. *Science* **2015**, *348*, 1234−1237.

(4) Noh, J. H.; Im, S. H.; Heo, J. H.; Mandal, T. N.; Seok, S. I. Chemical Management for Colorful, Efficient, and Stable Inorganic−Organic Hybrid Nanostructured Solar Cells. *Nano Lett.* **2013**, *13*, 1764−1769.

(5) Heo, J. H.; Im, S. H.; Noh, J. H.; Mandal, T. N.; Lim, C.-S.; Chang, J. A.; Lee, Y. H.; Kim, H.-j.; Sarkar, A.; Nazeeruddin Md, K.; Gratzel, M.; Seok, S. I. Efficient Inorganic-Organic Hybrid Heterojunction Solar Cells Containing Perovskite Compound and Polymeric Hole Conductors. *Nat. Photonics* **2013**, *7*, 486−491.

(6) Stranks, S. D.; Eperon, G. E.; Grancini, G.; Menelaou, C.; Alcocer, M. J. P.; Leijtens, T.; Herz, L. M.; Petrozza, A.; Snaith, H. J. Electron-Hole Diffusion Lengths Exceeding 1 Micrometer in an Organometal Trihalide Perovskite Absorber. *Science* **2013**, *342*, 341−344.

(7) Xing, G.; Mathews, N.; Sun, S.; Lim, S. S.; Lam, Y. M.; Grätzel, M.; Mhaisalkar, S.; Sum, T. C. Long-Range Balanced Electron- and Hole-Transport Lengths in Organic-Inorganic $CH_3NH_3PbI_3$. *Science* **2013**, *342*, 344−347.

(8) Jeon, N. J.; Noh, J. H.; Kim, Y. C.; Yang, W. S.; Ryu, S.; Seok, S. I. Solvent Engineering for High-Performance Inorganic−Organic Hybrid Perovskite Solar Cells. *Nat. Mater.* **2014**, *13*, 897−903.




DOI: 10.1021/acsami.7b09803
*ACS Appl. Mater. Interfaces* 2017, 9, 31950−31958

(9) Jeon, N. J.; Noh, J. H.; Yang, W. S.; Kim, Y. C.; Ryu, S.; Seo, J.; Seok, S. I. Compositional Engineering of Perovskite Materials for High-Performance Solar Cells. *Nature* **2015**, *517*, 476−480.
(10) Im, J.-H.; Jang, I.-H.; Pellet, N.; Grätzel, M.; Park, N.-G. Growth of $CH_3NH_3PbI_3$ Cuboids with Controlled Size for High-Efficiency Perovskite Solar Cells. *Nat. Nanotechnol.* **2014**, *9*, 927−932.
(11) Zhou, H.; Chen, Q.; Li, G.; Luo, S.; Song, T.-b.; Duan, H.-S.; Hong, Z.; You, J.; Liu, Y.; Yang, Y. Interface Engineering of Highly Efficient Perovskite Solar Cells. *Science* **2014**, *345*, 542−546.
(12) Yu, Z.; Sun, L. Recent Progress on Hole-Transporting Materials for Emerging Organometal Halide Perovskite Solar Cells. *Adv. Energy Mater.* **2015**, *5*, No. 1500213.
(13) NREL Best Research-Cell Efficiencies. https://www.nrel.gov/pv/assets/images/efficiency-chart.png (accessed May 23, 2017).
(14) Li, H.; Fu, K.; Boix, P. P.; Wong, L. H.; Hagfeldt, A.; Grätzel, M.; Mhaisalkar, S. G.; Grimsdale, A. C. Hole-Transporting Small Molecules Based on Thiophene Cores for High Efficiency Perovskite Solar Cells. *ChemSusChem* **2014**, *7*, 3420−3425.
(15) Li, H.; Fu, K.; Hagfeldt, A.; Grätzel, M.; Mhaisalkar, S. G.; Grimsdale, A. C. A Simple 3,4-Ethylenedioxythiophene Based Hole-Transporting Material for Perovskite Solar Cells. *Angew. Chem., Int. Ed.* **2014**, *53*, 4085−4088.
(16) Qin, P.; Paek, S.; Dar, M. I.; Pellet, N.; Ko, J.; Grätzel, M.; Nazeeruddin, M. K. Perovskite Solar Cells with 12.8% Efficiency by Using Conjugated Quinolizino Acridine Based Hole Transporting Material. *J. Am. Chem. Soc.* **2014**, *136*, 8516−8519.
(17) Ahn, N.; Son, D.-Y.; Jang, I.-H.; Kang, S. M.; Choi, M.; Park, N.-G. Highly Reproducible Perovskite Solar Cells with Average Efficiency of 18.3% and Best Efficiency of 19.7% Fabricated via Lewis Base Adduct of Lead(II) Iodide. *J. Am. Chem. Soc.* **2015**, *137*, 8696−8699.
(18) Hameiri, Z.; Mahboubi Soufiani, A.; Juhl, M. K.; Jiang, L.; Huang, F.; Cheng, Y.-B.; Kampwerth, H.; Weber, J. W.; Green, M. A.; Trupke, T. Photoluminescence and Electroluminescence Imaging of Perovskite Solar Cells. *Prog. Photovoltaics* **2015**, *23*, 1697−1705.
(19) Su, P.-Y.; Huang, L.-B.; Liu, J.-M.; Chen, Y.-F.; Xiao, L.-M.; Kuang, D.-B.; Mayor, M.; Su, C.-Y. A Multifunctional Poly-N-vinylcarbazole Interlayer in Perovskite Solar Cells For High Stability and Efficiency: A Test with New Triazatruxene-Based Hole Transporting Materials. *J. Mater. Chem. A* **2017**, *5*, 1913−1918.
(20) Saliba, M.; Orlandi, S.; Matsui, T.; Aghazada, S.; Cavazzini, M.; Correa-Baena, J.-P.; Gao, P.; Scopelliti, R.; Mosconi, E.; Dahmen, K.-H.; De Angelis, F.; Abate, A.; Hagfeldt, A.; Pozzi, G.; Graetzel, M.; Nazeeruddin, M. K. A Molecularly Engineered Hole-Transporting Material for Efficient Perovskite Solar Cells. *Nat. Energy* **2016**, *1*, No. 15017.
(21) Kumar, C. V.; Sfyri, G.; Raptis, D.; Stathatos, E.; Lianos, P. Perovskite Solar Cell with Low Cost Cu-phthalocyanine as Hole Transporting Material. *RSC Adv.* **2015**, *5*, 3786−3791.
(22) Javier Ramos, F.; Ince, M.; Urbani, M.; Abate, A.; Gratzel, M.; Ahmad, S.; Torres, T.; Nazeeruddin, M. K. Non-aggregated Zn(ii)-octa(2,6-diphenylphenoxy) Phthalocyanine as a Hole Transporting Material for Efficient Perovskite Solar Cells. *Dalton Trans.* **2015**, *44*, 10847−10851.
(23) Cheng, M.; Li, Y.; Safdari, M.; Chen, C.; Liu, P.; Kloo, L.; Sun, L. Efficient Perovskite Solar Cells Based on a Solution Processable Nickel(II) Phthalocyanine and Vanadium Oxide Integrated Hole Transport Layer. *Adv. Energy Mater.* **2017**, No. 1602556.
(24) Jiang, X.; Yu, Z.; Lai, J.; Zhang, Y.; Hu, M.; Lei, N.; Wang, D.; Yang, X.; Sun, L. Interfacial Engineering of Perovskite Solar Cells by Employing a Hydrophobic Copper Phthalocyanine Derivative as Hole-Transporting Material with Improved Performance and Stability. *ChemSusChem* **2017**, *10*, 1838−1845.
(25) Ke, W.; Zhao, D.; Grice, C. R.; Cimaroli, A. J.; Fang, G.; Yan, Y. Efficient Fully-Vacuum-Processed Perovskite Solar Cells Using Copper Phthalocyanine as Hole Selective Layers. *J. Mater. Chem. A* **2015**, *3*, 23888−23894.
(26) Sfyri, G.; Chen, Q.; Lin, Y.-W.; Wang, Y.-L.; Nouri, E.; Xu, Z.-X.; Lianos, P. Soluble Butyl Substituted Copper Phthalocyanine as Alternative Hole-Transporting Material for Solution Processed Perovskite Solar Cells. *Electrochim. Acta* **2016**, *212*, 929−933.
(27) Sfyri, G.; Kumar, C. V.; Wang, Y.-L.; Xu, Z.-X.; Krontiras, C. A.; Lianos, P. Tetra Methyl Substituted Cu(II) Phthalocyanine as Alternative Hole Transporting Material for Organometal Halide Perovskite Solar Cells. *Appl. Surf. Sci.* **2016**, *360*, 767−771.
(28) Qi, P.; Zhang, F.; Li, X.; Xiao, Y.; Guo, J.; Wang, S. 2,9,16,23-Tetrakis(7-coumarinoxy-4-methyl)- Metallophthalocyanines-Based Hole Transporting Material for Mixed-Perovskite Solar Cells. *Synth. Met.* **2017**, *226*, 1−6.
(29) Yang, G.; Wang, Y.-L.; Xu, J.-J.; Lei, H.-W.; Chen, C.; Shan, H.-Q.; Liu, X.-Y.; Xu, Z.-X.; Fang, G.-J. A Facile Molecularly Engineered Copper (II) Phthalocyanine as Hole Transport Material for Planar Perovskite Solar Cells with Enhanced Performance and Stability. *Nano Energy* **2017**, *31*, 322−330.
(30) Nouri, E.; Wang, Y.-L.; Chen, Q.; Xu, J.-J.; Paterakis, G.; Dracopoulos, V.; Xu, Z.-X.; Tasis, D.; Mohammadi, M. R.; Lianos, P. Introduction of Graphene Oxide as Buffer Layer in Perovskite Solar Cells and the Promotion of Soluble n-Butyl-substituted Copper Phthalocyanine as Efficient Hole Transporting Material. *Electrochim. Acta* **2017**, *233*, 36−43.
(31) Cho, K. T.; Trukhina, O.; Roldán-Carmona, C.; Ince, M.; Gratia, P.; Grancini, G.; Gao, P.; Marszalek, T.; Pisula, W.; Reddy, P. Y.; Torres, T.; Nazeeruddin, M. K. Molecularly Engineered Phthalocyanines as Hole-Transporting Materials in Perovskite Solar Cells Reaching Power Conversion Efficiency of 17.5%. *Adv. Energy Mater.* **2017**, *7*, No. 1601733.
(32) Li, M.; Li, Y.; Sasaki, S.-i.; Song, J.; Wang, C.; Tamiaki, H.; Tian, W.; Chen, G.; Miyasaka, T.; Wang, X.-F. Dopant-Free Zinc Chlorophyll Aggregates as an Efficient Biocompatible Hole Transporter for Perovskite Solar Cells. *ChemSusChem* **2016**, *9*, 2862−2869.
(33) Chou, H.-H.; Chiang, Y.-H.; Li, M.-H.; Shen, P.-S.; Wei, H.-J.; Mai, C.-L.; Chen, P.; Yeh, C.-Y. Zinc Porphyrin−Ethynylaniline Conjugates as Novel Hole-Transporting Materials for Perovskite Solar Cells with Power Conversion Efficiency of 16.6%. *ACS Energy Lett.* **2016**, *1*, 956−962.
(34) Chen, S.; Liu, P.; Hua, Y.; Li, Y.; Kloo, L.; Wang, X.; Ong, B.; Wong, W.-K.; Zhu, X. Study of Arylamine-Substituted Porphyrins as Hole-Transporting Materials in High-Performance Perovskite Solar Cells. *ACS Appl. Mater. Interfaces* **2017**, *9*, 13231−13239.
(35) Christians, J. A.; Fung, R. C. M.; Kamat, P. V. An Inorganic Hole Conductor for Organo-Lead Halide Perovskite Solar Cells. Improved Hole Conductivity with Copper Iodide. *J. Am. Chem. Soc.* **2014**, *136*, 758−764.
(36) Qin, P.; Tanaka, S.; Ito, S.; Tetreault, N.; Manabe, K.; Nishino, H.; Nazeeruddin, M. K.; Grätzel, M. Inorganic Hole Conductor-Based Lead Halide Perovskite Solar Cells with 12.4% Conversion Efficiency. *Nat. Commun.* **2014**, *5*, No. 3834.
(37) Mei, A.; Li, X.; Liu, L.; Ku, Z.; Liu, T.; Rong, Y.; Xu, M.; Hu, M.; Chen, J.; Yang, Y.; Grätzel, M.; Han, H. A Hole-Conductor−Free, Fully Printable Mesoscopic Perovskite Solar Cell with High Stability. *Science* **2014**, *345*, 295−298.
(38) Dualeh, A.; Moehl, T.; Nazeeruddin, M. K.; Grätzel, M. Temperature Dependence of Transport Properties of Spiro-MeOTAD as a Hole Transport Material in Solid-State Dye-Sensitized Solar Cells. *ACS Nano* **2013**, *7*, 2292−2301.
(39) Sfyri, G.; Kumar, C. V.; Sabapathi, G.; Giribabu, L.; Andrikopoulos, K. S.; Stathatos, E.; Lianos, P. Subphthalocyanine as Hole Transporting Material for Perovskite Solar Cells. *RSC Adv.* **2015**, *5*, 69813−69818.
(40) Zhang, F.; Yang, X.; Cheng, M.; Wang, W.; Sun, L. Boosting the Efficiency and the Stability of Low Cost Perovskite Solar Cells by Using CuPc Nanorods as Hole Transport Material and Carbon as Counter Electrode. *Nano Energy* **2016**, *20*, 108−116.
(41) Mane, S. B.; Hu, J.-Y.; Chang, Y.-C.; Luo, L.; Diau, E. W.-G.; Hung, C.-H. Novel Expanded Porphyrin Sensitized Solar Cells using Boryl Oxasmaragdyrin as the Sensitizer. *Chem. Commun.* **2013**, *49*, 6882−6884.


DOI: 10.1021/acsami.7b09803
*ACS Appl. Mater. Interfaces* 2017, 9, 31950−31958

(42) Mane, S. B.; Hung, C.-H. Molecular Engineering of Boryl Oxasmaragdyrins through Peripheral Modification: Structure−Efficiency Relationship. *Chem. - Eur. J.* **2015**, *21*, 4825−4841.
(43) Rajeswara Rao, M.; Ravikanth, M. Boron Complexes of Oxasmaragdyrin, a Core-Modified Expanded Porphyrin. *J. Org. Chem.* **2011**, *76*, 3582−3587.
(44) Poplavskyy, D.; Nelson, J. Nondispersive Hole Transport in Amorphous Films of Methoxy-Spirofluorene-Arylamine Organic Compound. *J. Appl. Phys.* **2003**, *93*, 341−346.
(45) Chu, T.-Y.; Song, O.-K. Hole Mobility of N,N′-bis(naphthalen-1-yl)-N,N′-bis(phenyl) Benzidine Investigated by using Space-Charge-Limited Currents. *Appl. Phys. Lett.* **2007**, *90*, No. 203512.
(46) Wang, Z. B.; Helander, M. G.; Greiner, M. T.; Qiu, J.; Lu, Z. H. Carrier Mobility of Organic Semiconductors Based on Current-Voltage Characteristics. *J. Appl. Phys.* **2010**, *107*, No. 034506.
(47) Ke, W.; Fang, G.; Liu, Q.; Xiong, L.; Qin, P.; Tao, H.; Wang, J.; Lei, H.; Li, B.; Wan, J.; Yang, G.; Yan, Y. Low-Temperature Solution-Processed Tin Oxide as an Alternative Electron Transporting Layer for Efficient Perovskite Solar Cells. *J. Am. Chem. Soc.* **2015**, *137*, 6730−6733.
(48) Rao, H.-S.; Chen, B.-X.; Li, W.-G.; Xu, Y.-F.; Chen, H.-Y.; Kuang, D.-B.; Su, C.-Y. Improving the Extraction of Photogenerated Electrons with SnO2 Nanocolloids for Efficient Planar Perovskite Solar Cells. *Adv. Funct. Mater.* **2015**, *25*, 7200−7207.


DOI: 10.1021/acsami.7b09803
*ACS Appl. Mater. Interfaces* 2017, 9, 31950−31958